ACS APPLIED MATERIALS & INTERFACES

Research Article

www.acsami.org

Simultaneous Detection of Tumor Cell Apoptosis Regulators Bcl-2 and Bax through a Dual-Signal-Marked Electrochemical Immunosensor

Shiwei Zhou, Yingying Wang, and Jun-Jie Zhu*

State Key Laboratory of Analytical Chemistry for Life Science, School of Chemistry & Chemical Engineering, Nanjing University, Nanjing 210093, P. R. China

Supporting Information

ABSTRACT: B-cell lymphoma 2 (Bcl-2) and Bcl-2-associated X protein (Bax) are often used to monitor the apoptosis of tumor cells and evaluate cancer drug effect. In this work, a novel sandwich-type dual-signal-marked electrochemical biosensor was fabricated for simultaneous detection of Bcl-2 and Bax proteins. Reduced graphene oxide (RGO) layers were used as substrate to immobilize Bcl-2 and Bax antibodies for further capturing target antigens. CdSeTe@CdS quantum dots (QDs) and Ag nanoclusters (NCs) with antibody modification and mesoporous silica amplification were used as signal probes, which were proportional to the amount of Bcl-2 and Bax antigens. Mesoporous SiO_2 can provide a larger surface area, more effectively charged by ethylene imine polymer or poly(diallyldimethylammonium chloride) to adsorb more probes. The Bcl-2 and Bax proteins were determined indirectly by the detection of oxidation peak currents of Cd and Ag using anodic stripping voltammetry, showing a good linear relationship in the protein concentration range from 1 ng/mL to 250 ng/mL. The detection limit of trace protein level was ~0.5 fmol. The biosensor was further introduced to investigate Bcl-2 and Bax expressions from nilotinib-treated chronic myeloid leukemia K562 cells. With the increase of drug dosage and incubation time, the up-regulation for Bax and down-regulation for Bcl-2 were observed, which indicated that the apoptosis level of K562 cells could be regulated by Bcl-2 family. The ratio of Bax/Bcl-2 was further calculated for evaluation of its drug effect and apoptosis level. The limited cell amount for detection reached less than 1×10^3 cells, much lower than traditional methods. Furthermore, completely independent detection step and stable acid solutions containing Ag^+ and Cd^{2+} for long-time storage contribute to reducing the error from the sample differences and avoiding the potential errors from the photodegradation of fluorescent probes, enzymolysis of DNA, or inactivation of enzyme during an excess experimental period.

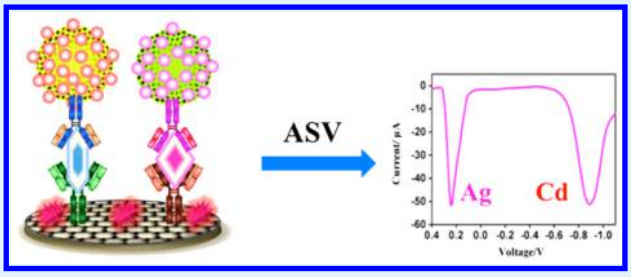

KEYWORDS: *Bcl-2, Bax, apoptosis, CML, electrochemical immunosensor*

INTRODUCTION

Apoptosis is a distinct physiological behavior essential to all the metazoans from the embryonic development to adult organisms' operation to maintain normal cellular homeostasis.[1] It plays an important role in cellular metabolism, especially in various diseases with characteristic increased or decreased cell survival.[2] The promotion or inhibition of apoptosis is adjusted by various apoptosis genes, in which B-cell lymphoma-2 (Bcl-2) family is one of the crucial regulators.[3−6] In Bcl-2 family, Bcl-2 (26 kDa) can effectively prevent apoptosis through several potential pathways including altering cell cycle rates, inhibiting oxidation, suppressing the release of Ca^{2+}, and interaction with Bcl-2-associated X protein (Bax, 21 kDa) as the heterodimers (Bcl-2-Bax).[2,7] Bax can promote apoptosis either through the generation of homodimers (Bax-Bax) or by promoting the release of cytochrome c.[8−10] When Bcl-2 is in excess of Bax and heterodimers (Bcl-2-Bax) dominate, cells are repressed to apoptosis; otherwise, the successful generation of homodimers (Bax-Bax) can promote the apoptosis.[11,12] The detection of Bcl-2 and Bax can also contribute to studying the apoptosis of tumor cells and determining the suitable therapeutic dose for various diseases.[13]

Chronic myeloid leukemia (CML) is a clonal disorder with massive clonal expansion of the myeloid lineage cells, resulting from the Bcr/Abl fusion gene.[14−16] Current therapies to CML include bone marrow transplantation, gene therapeutics, and chemotherapeutics, such as imatinib and interferon alfa.[17−21] Bone marrow transplantation is the most curative for CML, but subjected to the limited suitable donors, substantial morbidity, and mortality.[18] Interferon alfa has considerable side effects, even though it can prolong the survival of patients.[20] Imatinib, as the first generation of tyrosine kinase inhibitor, is gradually replaced by nilotinib and dasatinib, for its increasing drug-resistance.[21,22] So it is essential to evaluate the apoptosis of

Received: January 25, 2016
Accepted: March 6, 2016
Published: March 6, 2016

DOI: 10.1021/acsami.6b01010
ACS Appl. Mater. Interfaces 2016, 8, 7674−7682

CML cells and the drug effect of nilotinib to monitor the potential drug-resistance. Bcl-2 and Bax, as a pair of apoptosis-related genes and apoptotic regulators, can effectively reflect the apoptosis and clonal tendency of tumor cells.

The common technologies for Bcl-2 and Bax expression detection include flow cytometry (FCM),[23] gel electrophoresis,[24,25] Western blot,[26] and enzyme-linked immunesorbent assay (ELISA),[27] by fluorescence labeling, DNA transcription and amplification, or enzyme labeling methods. These technologies need precise instruments, complex sample processing, and high costs. Here, a simple and low cost sandwich dual-signal-marked electrochemical biosensor was first introduced for the simultaneous detection of Bcl-2 and Bax expressions, which could effectively reduce the errors from the sample differences.

To fabricate the biosensor (Scheme 1), some nanomaterials were prepared in advance for long-term storage, such as

Scheme 1. Fabrication of the Dual-Signal-Marked Electrochemical Immunosensor

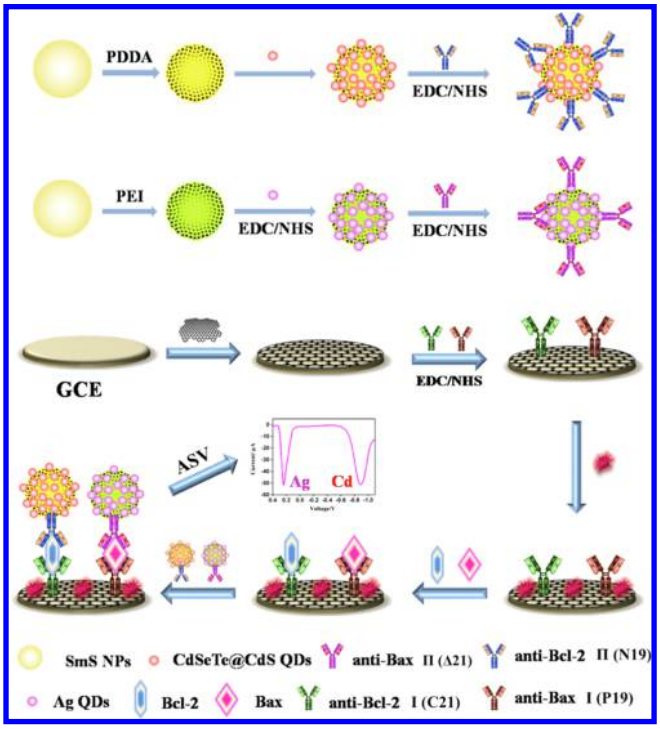

reduced graphene oxide (RGO),[28] silica nanoparticles (SiO_2),[29] Ag nanoclusters (NCs),[30] and CdSeTe@CdS quantum dots (QDs).[31] First, RGO was introduced as substrate on a glassy carbon electrode (GCE) to increase surface area and immobilize the antibodies.[32] After modification with antibodies I of Bcl-2, Bax, and block with bovine serum albumin (BSA) protein, the electrode was immersed into the mixed antigens to capture active Bcl-2 and Bax proteins. Finally, the electrode was further modified with antibody Π-targeted NCs (QDs) as the signal probes, which were proportional to antigens on the electrode. Ag NCs and CdSeTe@CdS QDs are easily prepared to get relatively uniform nanoparticles with regulated sizes. The excellent dispersion property and bundant functional groups also make them more convenient to be modified with antibodies. To amplify the signal, SiO_2 NPs were introduced as the carriers to enrich Ag NCs and CdSeTe@CdS QDs before antibody modification. Mesoporous SiO_2 (SiO_2@mSiO_2 or SmS) can provide a rougher surface and larger surface area, and thus can be more effectively charged by PEI or PDDA to adsorb more probes and antibodies. The as-expected biosensor, GCE/RGO/antibody-I/BSA/antigen/antibody-Π-NCs(QDs)-SmS, was then dissolved into the acid solution to obtain the corresponding Ag^+ and Cd^{2+}, and detected by anodic stripping voltammetry (ASV). The amount of Bax and Bcl-2 proteins were indirectly detected, which were proportional to the intensity of oxidation peak currents of Ag and Cd.

Nanoparticle-based electrochemical biosensors for the detection of proteins or cells were reported early in the last century.[33] Antibodies were captured by alkanethiols-modified gold surface for a nanoparticle-based electrochemical sandwich-type immunesensor.[34] On the basis of this, multidetection of proteins was then developed, meeting the demands of clinical diagnostics or applications. Joseph Wang reported a multiplexed immumoassay for simultaneous detection of at most four proteins, and the dual-detection limit reached ~3.3 and ~7.5 fmol.[35] Another of his works reported a quantum dot/aptamer-based dual-analyte electrochemical biosensor, which added fresh thrombin and lysozyme standard samples instead of quantum dots-modified proteins on the substrate, reaching a detection limit at ~0.05 fmol.[36] Similarly, Xu et al. reported a simultaneous detection for cancer cells and drug with a detection limit of ~5 ng/mL cells and ~50 μg/mL drug.[37] Recently, Joseph Wang also reported a simultaneous electrochemical measurement for metal and organic pollutants.[38] Compared with these reports, the dual-signal-marked electrochemical immunosensor in this work realized a low detection limit at ~0.5 fmol, only a little higher than the thrombin and lysozyme detection Wang reported, based on different work mechanisms. Furthermore, the completely independent detection step and the stable acid solutions containing Ag^+ and Cd^{2+} for long-term storage, contribute to avoiding the potential errors from the photodegradation of fluorescent probes, enzymolysis of DNA, or inactivation of enzyme during an excess experimental period.

The Bcl-2 and Bax protein expressions from K562 CML cells treated with nilotinib were investigated using the biosensor. The increase of drug dosage and incubation time resulted in an increase of Bax expression and a decrease of Bcl-2 expression, indicating an increasing amount of apoptotic cells. Meanwhile, excess drug dosage and overlong incubation time might lead to a fall-back of Bax and a rebound of Bcl-2 expression. Due to the diametrically opposite functions and interactions between Bcl-2 and Bax, the ratio of Bax/Bcl-2 was calculated for further evaluation of tumor cells apoptosis. The biosensor, introduced for the clinical detection of Bcl-2 and Bax expressions in cancer cells, reached a detection limit at ~1×10^3 cells, much lower than FCM (~10^4 cells),[39] Western blot (~10^5 cells),[40] and ELISA (~10^4 cells)[41] in some reports. This biosensor with the low detection limit could reduce errors from sample differences, improve the efficiency of the analysis with limited cell amount, and further contribute to monitoring the apoptosis of tumor cells and exploring a suitable drug dosage and drug delivery cycle for disease treament.

EXPERIMENTAL SECTION

Materials and Reagents. Cadmium chloride ($CdCl_2 \cdot 2.5H_2O$) was purchased from JinshanTingxin Chemical Reagent Co., Ltd. (Shanghai, China). Silver nitrate ($AgNO_3$), trisodium citrate dihydrate ($Na_3C_6H_5O_7 \cdot 2H_2O$), ammonium hydroxide ($NH_3 \cdot H_2O$) were all purchased from Nanjing Chemical Co., Ltd. (China). Graphite powder

DOI: 10.1021/acsami.6b01010
ACS Appl. Mater. Interfaces 2016, 8, 7674−7682

was obtained from J&K Scientific Co., Ltd. (Beijing, China). Mercury chloride ($HgCl_2$) was purchased from Jiangsu Donggong Chemicals (China). Selenium (Se) powder and Tellurium (Te) powder were purchased from Xinlongdiye Technology Co., Ltd. (Sichuan, China). Polymethacrylic acid sodium salt (PMAA, M_w 4000−6000, 40 wt % aqueous solution), 3-mercaptopropionic acid (MPA), 1-ethyl-3-(3-(dimethylamino)propyl) carbodiimide (EDC), *N*-hydroxysuccinimide (NHS), poly(diallyldimethylammonium chloride) (PDDA, M_w 100 000−200 000, 20 wt %), bovine serum albumin (BSA), sodium borohydride ($NaBH_4$), tetraethyl orthosilicate (TEOS), and hexadecyltrimethylammonium bromide (CTAB) were purchased from Sigma-Aldrich. Ethylene imine polymer (PEI, 99%, 10 000) was purchased from Aladdin. RIPA cell lysates was obtained from Beyotime Institute of Biotechnology (China). A caspase-3 cell activity detection kit and human K562 cells were purchased from Nanjing Keygen Biotech. Co. Ltd. (Jiangsu, China). Nilotinib was purchased from the Far Top Limited Co., Ltd. (Nanjing, Jiangsu, China). Anti-Bcl-2 (C21 and N19), and anti-Bax (P12 and Δ21) were purchased from Santa Cruz Biotechnology Co., Ltd. (Shanghai, China). Bcl-2 and Bax proteins were purchased from Beijing Biosynthesis Biotechnology Co., Ltd. (Beijing, China). All other reagents were of analytical grade and were used without further purification. All aqueous solutions were prepared using ultrapure water (Milli-Q, Millipore).

Phosphate buffered saline (PBS) buffer (0.1 M, pH 7.4) was prepared by mixing NaH_2PO_4 and Na_2HPO_4 with a certain mass ratio. HAc-NAc buffer (0.2 M, pH 5.2) was prepared with sodium acetate (NaAc) and acetic acid (HAc) with a certain mass ratio. K562 cells were cultured with RPMI 1640 medium (Giboc, Grand Island, NY) containing 10% fetal calf serum, and 100 μg/mL penicillin and streptomycin.[42]

Instruments. The fluorescence of Ag NCs and CdSeTe@CdS QDs was measured by a Bruker RF-5301PC fluorescence spectrometer. UV−vis absorption spectra were recorded by an UV-3600 spectral photometer (Shimadzu, Japan). Fourier transform infrared (FTIR) spectra were measured by a Bruker Vector 22 spectrometer. Scanning electron microscope (SEM) images and energy-dispersive X-ray spectrometry (EDX) were investigated with an S-4800 scanning electron microscope. Transmission electron micrographs (TEM) were observed by a JEOL JEM 200CX transmission electron microscope. High-resolution transmission electron microscopy (HRTEM) images were measured by a JEOL 2010 electron microscope. Caspase-3 cell activity detection kit by colorimetric analysis was detected at 405 nm with a Bio-Rad 680 microplate reader. Zeta Potential was taken on a nano-z zeta potential analyzer. A 500 W Xe lamp was used for preparation of Ag QDs. ASV signal was recorded on a CHI 660D electrochemical workstation (Shanghai Chenhua Apparatus Corporation, China). In the electrochemical system, a bare GCE electrode (Shanghai Chenhua Apparatus Corporation, China) was used as the working electrode, with a Pt wire as the counter electrode, and a saturated calomel electrode (SCE) as the reference electrode.

Synthesis of Ag NCs and Core−Shell CdSeTe@CdS QDs. Ag NCs were prepared as the reference reported.[30] 200 μL of PMAA solution (40%) was added into 4 mL of 50 mg/mL $AgNO_3$ aqueous solution, getting a transparent homogeneous solution after vigorous stirring. Then the solution was irradiated with a 500 W Xe lamp for 90s under evenly stirring until the color of the solution turned to dark fuchsia. The as-prepared Ag NCs were added into 10 mL of ethanol, incubated for 5 h, and finally the precipitate was redispersed into 4 mL of ultrapure water.

CdSeTe@CdS QDs were prepared by the reported method.[31] Under N_2 atmosphere, 50 mL of 5 mM $CdCl_2$ solution and 37 μL of MPA were mixed and stirred at the temperature below 10 °C after adjusting the pH to 12.2. Then freshly premixed NaHTe (104 μmol) and NaHSe (21 μmol) solution was added into above $CdCl_2$ solution rapidly with vigorous stirring for 2 h. Finally, the obtained CdSeTe clusters were purified with ethanol as mentioned above.

Another $CdCl_2$ solution and 40 μL of MPA were added into above CdSeTe solution, keeping the final concentration of Cd^{2+} at 5 mM. After the pH was tuned to 12.2 again, the mixed solution was irradiated and refluxed under microwave for 10 min. The as-prepared CdSeTe@CdS QDs were purified by precipitation with ethanol and redispersed in 50 mL of ultrapure water.

Synthesis of Reduced Graphene Oxide. Reduced graphene oxide (RGO) was synthesized by the reduction of graphene oxide (GO).[43,44] GO was prepared by a Hummers method as reported.[28,45] Then 25 mg of GO was dispersed into 100 mL ultrapure water. 1.0 g of sodium citrate was added after the solution was heated to 95 °C. After being stirred vigorously for 4 h, the precipitant was washed and centrifuged at 9500 r/min 3 times to get a homogeneous dispersed supernatant. The concentration of the RGO dispersion was measured through a drying and weighing method.

Synthesis of SmS NPs. Solid SiO_2 spheres were synthesized by the hydrolysis of TEOS.[29] First, 2.5 mL of $NH_3{\cdot}H_2O$ (28 wt %) was added into 50 mL of absolute ethanol. After being stirred for 30 min, 1.5 mL of TEOS (98%) was slowly added into the solution and stirred for 24 h. The obtained SiO_2 spheres were washed with ethanol and centrifuged 3 times, and then dried at 70 °C. To coat with the mesoporous silica shell, 100 mg of the above-prepared SiO_2 spheres were dispersed into 7.5 mL aqueous solution, containing 40 mg of CTAB and 3.15 mL of ethanol, and then sonicated and stirred vigorously for 30 min. Then 113 μL of $NH_3{\cdot}H_2O$ and 75 μL of TEOS were successively added into the mixture solution and stirred for 12 h. The as-expected SmS NPs suspension was washed with ethanol, centrifuged, and dried at 70 °C.[29] To remove the residual CTAB, 40 μL of hydrochloric acid (HCl) was added into the ethanol dispersion containing 100 mg of SmS NPs, and then stirred for 3 h at 60 °C.[46] After being washed twice with ethanol, SmS NPs were redispersed into 10 mL of ethanol for use.

Fabrication of Antibody Π-NCs(QDs)-SmS Probes. NCs-(QDs)-SmS composites were prepared as the signal probes. First, 5 mg of SmS NPs were dispersed into 5 mL of 1 wt % PDDA or PEI solution and sonicated for 30 min. After washed with ultrapure water for 3 times, the PDDA-modified SmS NPs were redispersed into CdSeTe@CdS QDs solution (5 mL), and the PEI-modified SmS NPs were redispersed into Ag NCs solution (5 mL). Ag NCs were preactivated with 2 mg of EDC and 1 mg of NHS for 30 min at room temperature. The solution was sonicated for 10 min and then centrifuged to remove residual QDs and NCs. Repeat modification with QDs or NCs for twice. The obtained composites were washed with ultrapure water for 3 times and redispersed into 5 mL of PBS containing 10 mg of EDC and 5 mg of NHS for 30 min to active the carboxyl groups. Then 50 μg of anti-Bcl-2 (N19) and 50 μg of anti-Bax (Δ21) were separately added into the expected Cd-SmS and Ag-SmS composites in PBS (5 mL) after removing residual EDC and NHS. Then the solution was incubated and vibrated overnight. Finally, the antibody Π-targeted composites were washed with PBS containing 0.1 wt % Tween 20 for three times and redispersed into 2.5 mL of PBS for further use. Tween 20 was used to block the composites to reduce the nonspecific absorption with the biosensor and improve the dispersion of the probes in the solution in addition.

Fabrication of the Electrochemical Biosensor. The electrochemical biosensor was fabricated on a glassy carbon electrode (GCE). Briefly, 10 μL of RGO dispersion (1 mg/mL) was dropped on the GC electrode and dried at room temperature. The RGO substrate could increase the surface area due to the folds and could effectively immobilize the antibodies.[32] Then the electrode was immersed into 100 μL of PBS containing 0.2 mg EDC and 0.1 mg NHS for 30 min, and washed with PBS for twice. After that, 10 μL of antibody mixture containing 10 μg/mL anti-Bcl-2 (C21) and 10 μg/mL anti-Bax (P19) was dropped onto the modified electrode and incubated for 12 h at 4 °C in 100% humidity. After being washed with PBS, the electrode was immersed into 100 μL of PBS solution containing 1 mg/mL BSA for 1.0 h to block the residual active sites and then washed with PBS. The electrode was further incubated with 10 μL of standard solutions or cell lysates containing different concentrations of Bcl-2 and Bax antigens for 1.5 h at 37 °C in 100% humidity. Before that, 2 μL of dithiothreitol (DTT) solution was added into the antigen mixture to inhibit the generation of dimers. After being washed twice to remove the residual antigens, the electrode was immersed into 10 μL of signal

DOI: 10.1021/acsami.6b01010
ACS Appl. Mater. Interfaces 2016, 8, 7674−7682

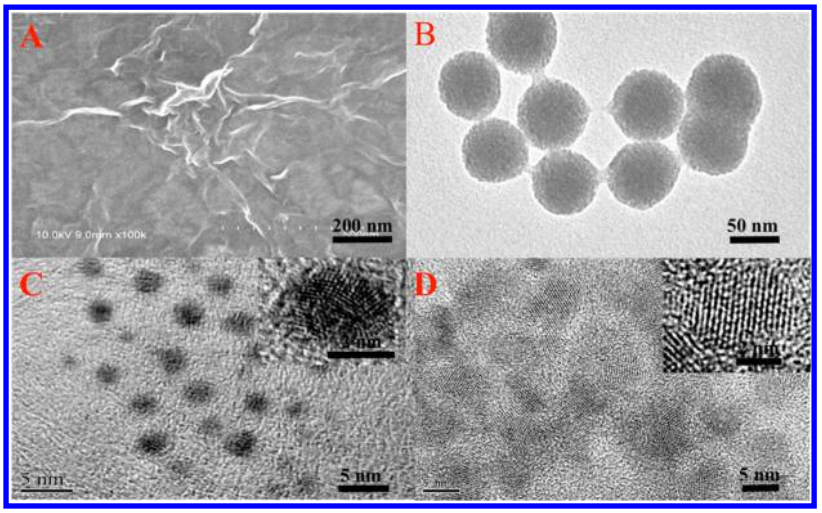

Figure 1. (A) SEM image of reduced graphene oxide, (B) TEM image of SmS NPs, (C) HRTEM image of Ag NCs, and (D) HRTEM image of CdSeTe@CdS QDs.

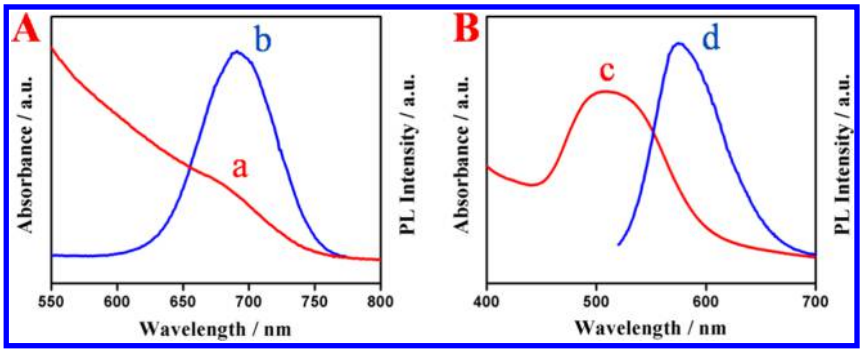

Figure 2. (A) UV−vis absorption spectrum (a) and photoluminescence (PL) spectrum (b) of CdSeTe@CdS QDs; (B) UV−vis absorption spectrum (c) and photoluminescence (PL) spectrum (d) of Ag NCs. The excitation wavelength was chosen as 500 nm for the PL detection of Ag NCs and CdSeTe@CdS QDs.

probes dispersion for 2 h at 37 °C in 100% humidity. The probe dispersion contained 1 mg/mL Δ21−Ag−SmS and 1 mg/mL N19-Cd-SmS composites. After finally being washed with PBS to remove nonspecifically bounded nanoprobes, the electrode was immersed into 200 μL of HNO_3 solution (0.1 M) for 2 h to dissolve the probes. The resulting solution was mixed with HAc-NAc buffer (4.8 mL, 0.2 M, pH 5.2) containing 40 μg/mL Hg^{2+} and 10 ug/mL KNO_3 for the detection of metal ions by ASV. The detection was carried out under N_2 atmosphere by electrode position at −1.1 V for 12 min with mild stirring, then standing for 2 min, and finally stripping from −1.1 to 0.5 V with a square-wave voltammetric waveform. The potential step was 4 mV, the frequency was 25 Hz, and the amplitude was 25 mV.

Inducing the Apoptosis of K562 Cells with Nilotinib. K562 cells were one of the human CML cells, which were chosen to study Bcl-2 and Bax protein expressions induced by the target antileukemia drug, nilotinib. During the apoptosis, 4 mL of 5×10^5 mL^{-1} K562 cells was treated with 30 μM nilotinib for 0, 8, 16, 24, and 32 h respectively, and then washed for twice with PBS. These induced cells were dissolved and lysed into 200 μL of ice-cold RIPA lysates containing 2 μL DTT for 30 min, and then centrifuged with 13 000 r/m for 15 min at 4 °C, getting a supernatant of Bcl-2 and Bax proteins. Before use, the supernatant was stored at −80 °C. Similarly, nilotinib was also used to induce the apoptosis of K562 cells at different concentrations of 0, 10, 20, 30, 40, and 50 μM for 16 h.

RESULTS AND DISCUSSION

Characterization of RGO Substrate and Signal Probes. RGO is often used as the substrate material for its good conductivity, large surface area, and π−π conjugate structure.[47,48] In the SEM image of Figure 1A, RGO showed a relatively flat structure, which was suitable for the modification of GC electrode. Its absorption ability[32] and carboxyl groups also contributed to the immobilization of antibodies with abundant amino groups. Figure S1 showed the Fourier Transform Infrared Spectroscopy (FTIR) absorption spectra (KBr) of GO and RGO.[49] GO showed two obvious peaks at ∼3400 and 3200 cm^{-1}, corresponding to the stretching O—H and broad coupling O—H bond. The characteristic peak of O—H from carboxyl was observed at ∼1400 cm^{-1}. RGO showed weaker absorption peaks of O—H, indicating the reducing O—H groups on the layer surface. The absorption peaks of C═O, C═C, C—O, and C—O—C bonds were separately observed at ∼1700, ∼1600, ∼1050, and ∼1220 cm^{-1} in both GO and RGO spectra. These much weaker peaks for the latter demonstrated the successful reduction of GO with less functional groups, which could improve the conductivity and π−π conjugate capacity of RGO. The TEM image in Figure 1B showed that SmS NPs were homogeneously spherical with a diameter of ∼60 nm and a mesoporous shell of ∼10 nm, while the solid SiO_2 core with a diameter of ∼40 nm was shown in Figure S2. The mesoporous structure can provide a rougher surface and larger surface area, and thus can be more effectively charged by PEI or PDDA. SmS NPs, introduced as the carriers for signal amplification, can effectively improve the sensitivity and detection limit. Figure 1C, D showed the HRTEM images of Ag NCs and CdSeTe@CdS QDs. Ag NCs were spherical

DOI: 10.1021/acsami.6b01010
ACS Appl. Mater. Interfaces 2016, 8, 7674−7682

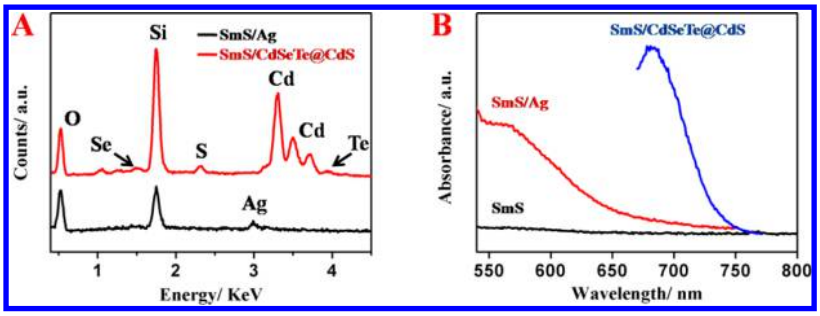

Figure 3. (A) EDX analysis of Ag-SmS and Cd-SmS; (B) photoluminescence (PL) spectra of SmS, Ag-SmS, and Cd-SmS. The excitation wavelength was chosen as 500 nm for the PL detection.

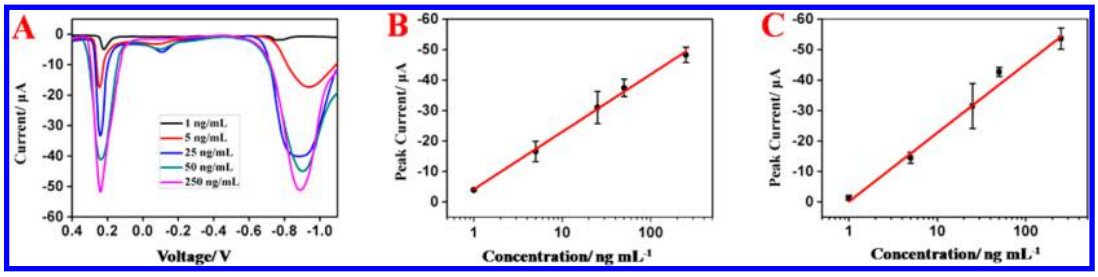

Figure 4. (A) The typical ASV responses with different concentrations of Bcl-2 and Bax proteins on the electrochemical biosensor; (B) calibration curve between the oxidation peak current of Ag and the concentration of Bax; and (C) calibration curve between the oxidation peak current of Cd and the concentration of Bcl-2.

with clear sequential lattice fringes. The average diameter was ~4 nm, and the lattice spacing was ~0.13 nm. An average diameter of ~5 nm with lattice spacing of ~0.3 nm was also observed on the CdSeTe@CdS QDs. The size difference to SmS NPs indicated Ag NCs and CdSeTe@CdS QDs could be enriched on the SmS NPs for signal amplication.

The Zeta Potential in Figure S3 showed that PDDA or PEI-modified SmS NPs were positive charged, while Ag NCs and CdSeTe@CdS QDs were negative charged. The reduced zeta potential of the composites indicated the successful modification of SmS NPs with the Ag NCs and CdSeTe@CdS QDs. Ag NCs modified with PMAA molecules could effectively improve the dispersion of Ag QDs, inhibiting the agglomeration and adsorption to SmS NPs as the long-chain structure of PMAA molecules with abundant carboxyl groups. Thus, the preparation of Ag-SmS composites by amide reaction was chosen as a better method, instead of electrostatic adsorption. In contrast, Cd-SmS composites were prepared by electrostatic adsorption for the small structure of MPA molecules, which could not inhibit the adsorption to SmS NPs. UV−vis absorption spectra and photoluminescence (PL) spectra for Ag NCs and CdSeTe@CdS QDs were shown in Figure 2. A characteristic UV−vis absorption peak of CdSeTe@CdS QDs was observed at ~670 nm, while the emission PL peak located at ~690 nm. The absorption and emission peak of Ag NCs were observed at ~510 nm and ~580 nm, respectively. After bounded with SmS NPs, the composites still showed similar characteristic PL peaks (Figure 3B). It indicated the successful synthesis of these composites without obvious structure change. The EDX analysis of these two composites (Figure 3A) also showed characteristic peaks of Cd, Se, Te, S, and Ag elements separately, indicating that the metal ions from the probes could be detected by ASV. After modification with antibody Π, the hydrophily of the composites showed little decrease due to the hydrophobicity of the antibodies. It is worth mentioning that the carboxyl groups on the composites can combine with the amino groups either on the fragment antigen binding region (Fab) or on the fragment crystallizable region (Fc) of antibodies. The Fc region is more hydrophobic than the Fab region. Thus, the combined probability between the carboxyl groups and the amino groups on the Fc region is much higher, for the hydrophobic surface of the composites. The antibody-modified probes with exposed Fab region could also effectively combine with the antigens on the biosensor.

Detection of Bcl-2 and Bax Proteins. The specifically captured signal probes are proportional to the amount of antigens immobilized on the electrode. Cd^{2+} and Ag^{+} ions from the probes could be detected by ASV after the probes were dissolved in HNO_3 solution. Thus, the intensity of oxidation peak currents of Cd and Ag are proportional to the amount of Bcl-2 and Bax antigens separately. Ag NCs and CdSeTe@CdS QDs are chosen as the signal probes, for their independent oxidation peaks without interference and the simple preparation process to get a relatively uniform and regulated size. The excellent dispersion property and abundant functional groups also make Ag NCs and CdSeTe@CdS QDs more convenient to be modified with biomolecules. Figure S4 shows that the oxidation peak of Ag is at ~0.3 V, while the oxidation peak of Cd is at ~−0.8 V. In order to investigate the performance of the biosensor, different concentrations of Bcl-2 and Bax standard samples were introduced to monitor the variation of amperemetric responses of Cd and Ag as shown in Figure 4. The intensity of peak currents of Cd and Ag showed a good linear relationship with the capacity of Bcl-2 and Bax on the electrode in a concentration range from 1 ng/mL to 250 ng/mL. The linear regression equations were $I_{Cd}(\mu A) = -0.13187 - 22.59216 \times \log C_{Bcl\text{-}2}(ng/mL)$ with a correlation coefficient R^2 of 0.9856, and $I_{Ag}(\mu A) = -4.16741 - 18.8774 \times \log C_{Bax}(ng/mL)$ with R^2 of 0.9924. Thus, the electrochemical biosensor exhibited a good analytical performance for the detection of Bax and Bcl-2 expressions. It is worth noting that there is sometimes a small peak at ~−0.05 V, confirmed as the

DOI: 10.1021/acsami.6b01010
ACS Appl. Mater. Interfaces 2016, 8, 7674−7682

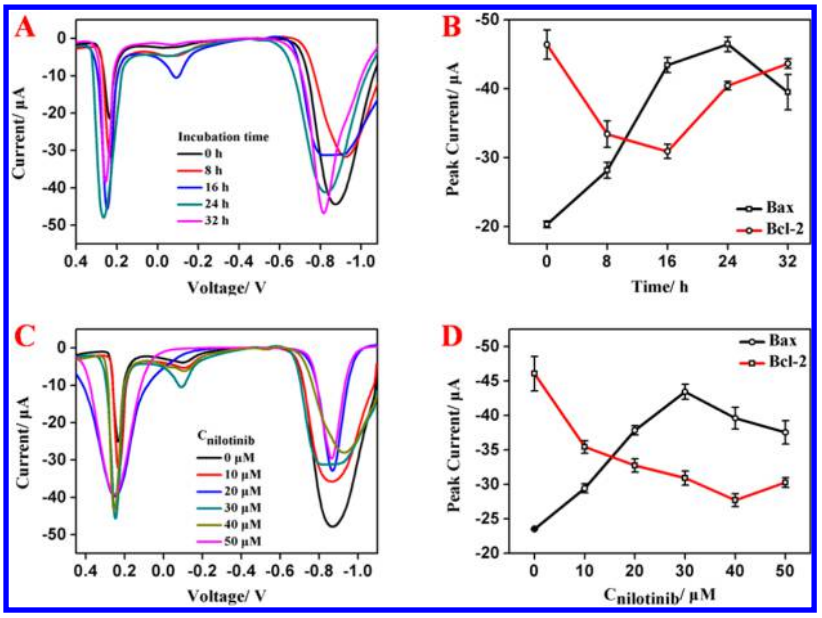

Figure 5. (A) The ASV response for active Bcl-2 and Bax proteins extracted from the K562 cells incubated with 30 μM nilotinib for different time; (B) the relationship between the peak currents for Bcl-2 and Bax and the incubation time of K562 cells with 30 μM nilotinib; (C) the ASV response for active Bcl-2 and Bax proteins extracted from the K562 cells incubated with different concentrations of nilotinib for 16 h; and (D) the relationship between the peak currents for Bcl-2 and Bax and the concentrations of nilotinib used to induce the K562 cells for 16 h.

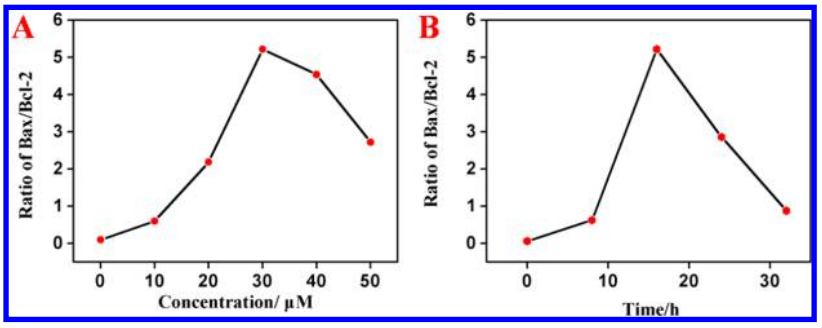

Figure 6. (A) The relationship between Bax/Bcl-2 ratio and the concentration of nilotinib, the incubation time was 16 h; (B) the relationship between Bax/Bcl-2 ratio and the incubation time, the drug dosage was 30 μM.

impurity Hg^{2+} ions from the $HgCl_2$. It is resulted from the response differences during the experiment, which actually would not disturb the detection.

Bcl-2 and Bax are a pair of apoptotic genes that can regulate the apoptosis of tumor cells, in which Bcl-2 is an antiapoptotic factor, and Bax is a pro-apoptotic factor. When Bax is in excess of Bcl-2, the tumor cells trend to be apoptotic. Otherwise, the cancer cells trend to be antiapoptotic. Figure 5 showed the amperometric response of Ag^{+} and Cd^{2+}, proportional to Bax and Bcl-2 protein expressions extracted from the K562 cells incubated with nilotinib. The response for Bax increased with the increasing drug concentration and incubation time until 30 μM and 24 h. In contrast, the response for Bcl-2 reduced with the increase of drug concentration and incubation time and returned back after 40 μM and 16 h. The increase of Bax and the decrease of Bcl-2 indicated nilotinib could effectively induce the aopotosis of K562 cells and inhibit cell proliferation. The subsequent decrease of Bax and increase of Bcl-2 may be caused by the drug toxicity with an excess drug dosage or drug inactivation for an overlong incubation time. The favorable signal-to-noise ASV response for the standard samples indicated a detection limit of ~1 ng/mL (0.5 fmol in 10-μL samples), corresponding to ~1×10^3 cells with highest Bcl-2 or Bax expressions. Some reports indicated a detection limit for Bcl-2 and Bax expressions by FCM with ~10^4 cells,[39] Western blot with ~10^5 cells,[40] or ELISA with ~10^4 cells.[41] Thus, the electrochemical immunosensor has a much lower detection limit for Bcl-2 and Bax expressions.

Since Bax and Bcl-2 can suppress each other with diametrically opposite functions, the increase of Bax or decrease of Bcl-2 expression can only show some evidence for evaluation of tumor cell apoptosis. In contrast, the ratio of Bax/Bcl-2, for its intuitive reflection of the dominant position of Bcl-2-Bax or Bax-Bax dimers, is more meaningful and more accurate to evaluate the apoptosis of tumor cells. Through conversion with the linear relationship shown in Figure 4, the concentrations of Bcl-2 and Bax protein expressions during the K562 cells treatment were easily calculated as shown in Table S1. The ratio of Bax/Bcl-2 was further calculated through these corresponding Bax and Bcl-2 expressions. Figure 6 showed that the ratio of Bax/Bcl-2 increased rapidly with the increasing drug dosage until 30 μM and incubation time less than 16 h, indicating the promotion of apoptosis. Continuing increasing the concentration of nilotinib or prolonging incubation time could lead to the decrease of the ratio, indicating the inhibition of apoptosis efficiency. When the ratio of Bax/Bcl-2 was over

DOI: 10.1021/acsami.6b01010
ACS Appl. Mater. Interfaces 2016, 8, 7674−7682

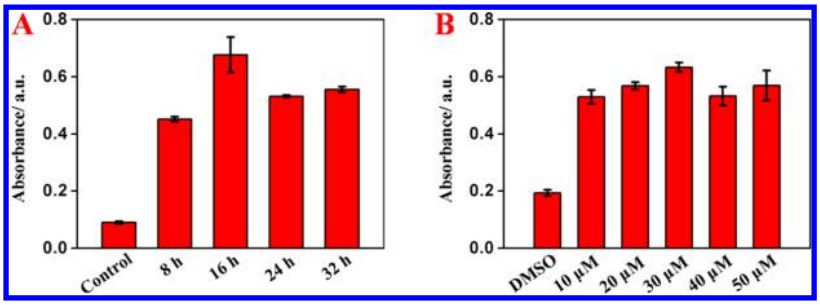

Figure 7. (A) Time course for caspase-3 activity extracted from K562 cells induced by 30 μM nilotinib for different time; (B) concentration-dependence for caspase-3 activity extracted from K562 cells induced by different concentrations of nilotinib for 16 h. The results were detected by a colorimetric method with a caspase-3 cellular activity assay kit.

1.0, the Bax-Bax homodimers would be dominantly generated to promote the apoptosis of K562 cells. Thus, nilotinib was considered to be effective for the treatment of K562 cells in a concentration range from 20 to 50 μM during an incubation time from 16 to 24 h. The increasing ratio of Bax/Bcl-2 indicated an improvement of apoptotic level, thus the optimal drug dosage was selected to be 30 μM, and the incubation time was selected as 16 h.

Bcl-2 family could effectively regulate the release of cytochrome c in the mitochondria. The pro-apoptotic proteins as Bax could promote the open of permeability transition pore (PT) in the mitochondria, and the antiapoptotic proteins as Bcl-2 inhibit this process instead. The opened PT pore will cause the decrease of mitochondrial transmembrane potential and lead to the release of cytochrome *c*. Meanwhile, the Bcl-2 family could also insert the mitochondrial membrane to generate large channels, and next release the cytochrome *c* from the mitochondria. Cytochrome *c* will further generate the apoptosome with other apoptotic proteins to active the key apoptosis marker—caspase-3, trigger caspase cascade reactions, and lead to the final apoptosis.[50,51] Thus, the expression levels of Bcl-2 and Bax proteins will directly regulate the activity of caspase-3, whereas caspase-3 could reflect the Bcl-2 and Bax expressions, and the apoptosis level of cancer cells. To verify the conclusion in Figure 6, caspase-3 was detected by a colorimetric method with a caspase-3 cellular activity assay kit[52] shown in Figure 7. It showed that the activity of caspase-3 increased to the maximum when K562 cells were induced by 30 μM nolotinib for 16 h, and then fell back afterward. The result indicated that the optimal drug dosage was 30 μM, and the incubation time was 16 h for apoptosis of K562 cells, corresponding to the result of the electrochemical detection for Bcl-2 and Bax. It indicated that the detection of Bcl-2 and Bax expressions could effectively be used to evaluate the apoptosis and monitor the drug effect. Actually, besides the Bcl-2 family as the major inducible factor, to some extent, some other apoptotic factors such as caspase-8 and calpain also could active caspase-3.[50] Thus, the expression of caspase-3 will only be integrally consistent with the result of Bax/Bcl-2 ratio, showing some slight differences. We can see that, different from the result of Bcl-2 and Bax expression detection, the expression of caspase-3 will decrease after keeping increasing the drug concentration to more than 30 μM or incubation time to more than 16 h, and increase again when K562 cells were induced with 50 μM of nolotinib or 32 h of incubation time. But, this slight difference has almost no influence on the evaluation of cell apoptosis and monitoring of drug effect. And in most cases, the activity of caspase-3 could still reflect the expression trend of Bcl-2 and Bax.

CONCLUSIONS

This work introduced a novel dual-signal-marked electrochemical sandwich immunosensor for the simultaneous detection of Bcl-2 and Bax proteins. RGO was used as substrate to immobilize the antibodies. The electrode next captured the corresponding antigens of Bax and Bcl-2, and further specifically recognized the antibody-Π-targeted signal probes. The signal probes with mesoporous SiO_2 amplification could improve the sensitivity and detection limit. The peak currents of Cd and Ag detected by ASV showed a proportional linear relationship in a concentration range of Bcl-2 and Bax proteins. It indicated the biosensor was suitable for the detection of Bcl-2 and Bax expressions. With this biosensor, the Bcl-2 and Bax from the apoptotic K562 cells treated with nilotinib was investigated. The increase of the drug dosage and incubation time could obviously increase Bax expression and reduce Bcl-2 expression. The rise of Bax/Bcl-2 ratio also indicated the promotion of the apoptosis of K562 cells. Although CML is caused by Bcr/Abl fusion gene, the apoptosis of CML cells regulated by Bcl-2 family can provide a potential synergistic therapy for the cancer treatment. The simultaneous detection of Bcl-2 and Bax expressions could reach a detection limit of ~0.5 fmol or ~1×10^3 cells, much lower than most of other similar biosensors and traditional methods for apoptosis proteins detection. Furthermore, the novel electrochemical immunosensor also provides a promising tool for apoptosis research and valid therapeutic schedule of other diseases. The simultaneous detection can reduce the errors from separated detection of Bcl-2 and Bax in different samples. The independent fabrication and detection steps and stable metal ions solution also benefit the experiment arrangement, reducing the potential errors of the photodegradation of fluorescence, enzymolysis of DNA, or inactivation of enzyme during an excess experimental period.

ASSOCIATED CONTENT

Supporting Information

The Supporting Information is available free of charge on the ACS Publications website at DOI: 10.1021/acsami.6b01010.

FTIR absorption spectra of GO and RGO, TEM image of solid SiO_2 nanoparticles, the Bax and Bcl-2 protein expressions from K562 cells treated with nilotinib, the zeta potential of the probes, and the ASV response comparison of bare GCE and signal probes (PDF)

AUTHOR INFORMATION

Corresponding Author

*E-mail: jjzhu@nju.edu.cn (J.-J.Z.).

DOI: 10.1021/acsami.6b01010
ACS Appl. Mater. Interfaces 2016, 8, 7674−7682

Notes

The authors declare no competing financial interest.

■ ACKNOWLEDGMENTS

The authors acknowledge financial support from the National Basic Research Program of China (2011CB933502), the National Natural Science Foundation of China (21335004). The authors are also thankful for the help of Ziyi Zhang from Nenan University.

■ REFERENCES

(1) Danial, N. N.; Korsmeyer, J. S. Cell Death: Critical Control Points. *Cell* **2004**, *116*, 205−219.
(2) Fleisher, T. A. Apoptosis. *Ann. Allergy, Asthma, Immunol.* **1997**, *78*, 245−249.
(3) Green, D. R.; Reed, J. C. Mitochondria and Apoptosis. *Science* **1998**, *281*, 1309−1312.
(4) Adams, J. M.; Cory, S. The Bcl-2 Protein Family: Arbiters of Cell Survival. *Science* **1998**, *281*, 1322−1326.
(5) Cory, S.; Adams, J. M. The BCL2 Family: Regulators of the Cellular Life-or-Death Switch. *Nat. Rev. Cancer* **2002**, *2*, 647−656.
(6) Youle, R. J.; Strasser, A. The BCL-2 Protein Family: Opposing Activities that Mediate Cell Death. *Nat. Rev. Mol. Cell Biol.* **2008**, *9*, 47−59.
(7) Correia, C.; Lee, S. H.; Meng, X. W.; Vincelette, N. D.; Knorr, K. L. B.; Ding, H. S.; Nowakowski, G. S.; Dai, H. M.; Kaufmann, S. H. Emerging Understanding of Bcl-2 Biology: Implications for Neoplastic Progression and Treatment. *Biochim. Biophys. Acta, Mol. Cell Res.* **2015**, *1853*, 1658−1671.
(8) Westphal, D.; Kluck, R. M.; Dewson, G. Building Blocks of the Apoptotic Pore: How Bax and Bak are Activated and Oligomerize during Apoptosis. *Cell Death Differ.* **2014**, *21*, 196−205.
(9) Renault, T. T.; Manon, S. Bax: Addressed to Kill. *Biochimie* **2011**, *93*, 1379−1391.
(10) Kumarswamy, R.; Chandna, S. Putative Partners in Bax Mediated Cytochrome-c Release: ANT, CypD, VDAC or None of Them? *Mitochondrion* **2009**, *9*, 1−8.
(11) Oltval, Z. N.; Milliman, C. L.; Korsmeyer, S. J. BCL-2 Heterodimerizes In-vivo with a Conserved Homolog, Bax, that Accelerates Programmed Cell-Death. *Cell* **1993**, *74*, 609−619.
(12) Williams, G. T.; Smith, C. A. Molecular Regulation of Apoptosis-Genetic-Controls on Cell-Death. *Cell* **1993**, *74*, 777−779.
(13) Xu, L. L.; Zhu, L.; Jia, N. M.; Huang, B. Z.; Tan, L.; Yang, S. F.; Tang, H.; Xie, Q. J.; Yao, S. Z. Quantification of Bax Protein on Tumor Cells Based on Electrochemical Immunoassay. *Sens. Actuators, B* **2013**, *186*, 506−514.
(14) Druker, B. J.; Talpaz, M.; Resta, D. J.; Peng, B.; Buchdunger, E.; Ford, J. M.; Lydon, N. B.; Kantarjian, H.; Capdeville, R.; Ohno-Jones, S.; Sawyers, C. L. Efficacy and Safety of a Specific Inhibitor of the BCR-ABL Tyrosine Kinase in Chronic Myeloid Leukemia. *N. Engl. J. Med.* **2001**, *344*, 1031−1037.
(15) Nowell, P. C.; Hungerford, D. A. Minute Chromosome in Human Chronic Granulocytic Leukemia. *Science* **1960**, *132*, 1497.
(16) Rowley, J. D. New Consistent Chromosomal Abnormality in Chronic Myelogenous Leukemia Identified by Quinacrine Fluorescence and Giemsa Staining. *Nature* **1973**, *243*, 290−293.
(17) Silver, R. T.; Woolf, S. H.; Hehlmann, R.; Appelbaum, F. R.; Anderson, J.; Bennett, C.; Goldman, J. M.; Guilhot, F.; Kantarjian, H. M.; Lichtin, A. E.; Talpaz, M.; Tura, S. An Evidence-based Analysis of the Effect of Busulfan, Hydroxyurea, Interferon, and Allogeneic Bone Marrow Transplantation in Treating the Chronic Phase of Chronic Myeloid Leukemia: Developed for the American Society of Hematology. *Blood* **1999**, *94*, 1517−1536.
(18) Barrett, A. J.; Ito, S. The Role of Stem Cell Transplantation for Chronic Myelogenous Leukemia in the 21st Century. *Blood* **2015**, *125*, 3230−3235.
(19) Gewirtz, A. M. Oligonucleotide Therapeutics: Clothing the Emperor. *Curr. Opin. Mol. Ther.* **1999**, *1*, 297−306.
(20) Hochhaus, A.; Reiter, A.; Saussele, S.; Reichert, A.; Emig, M.; Kaeda, J.; Schultheis, B.; Berger, U.; Shepherd, P. C. A.; Allan, N. C.; Hehlmann, R.; Goldman, J. M.; Cross, N. C. P. Molecular Heterogeneity in Complete Cytogenetic Responders after Interferon-alpha Therapy for Chronic Myelogenous Leukemia: Low Levels of Minimal Residual Disease are Associated with Continuing Remission. *Blood* **2000**, *95*, 62−66.
(21) Marce, S.; Cortes, M.; Zamora, L.; Cabezon, M.; Grau, J.; Milla, F.; Feliu, E. A Thirty-five Nucleotides BCR-ABL1 Insertion Mutation of Controversial Significance Confers Resistance to Imatinib in a Patient with Chronic Myeloid Leukemia (CML). *Exp. Mol. Pathol.* **2015**, *99*, 16−18.
(22) Griffin, J. D.; Guerin, A.; Chen, L.; Macalalad, A. R.; Luo, J. Y.; Ionescu-Ittu, R.; Wu, E. Q. Comparing Nilotinib with Dasatinib as Second-line Therapies in Patients with Chronic Myelogenous Leukemia Resistant or Intolerant to Imatinib — A Retrospective Chart Review Analysis. *Curr. Med. Res. Opin.* **2013**, *29*, 623−631.
(23) Boersma, A. W. M.; Nooter, K.; Burger, H.; Kortland, C. J.; Stoter, G. Bax Upregulation is an Early Event in Cisplatin-induced Apoptosis in Human Testicular Germ-cell Tumor Cell Line NT2, as Quantitated by Flow Cytometry. *Cytometry* **1997**, *27*, 275−282.
(24) Hu, Z. B.; Minden, M. D.; McCulloch, E. A. Phosphorylation of Bcl-2 after Exposure of Human Leukemic Cells to Retinoic Acid. *Blood* **1998**, *92*, 1768−1775.
(25) Thomas, A.; ElRouby, S.; Reed, J. C.; Krajewski, S.; Silber, R.; Potmesil, M.; Newcomb, E. W. Drug-induced Apoptosis in B-cell Chronic Lymphocytic Leukemia: Relationship between p53 Gene Mutation and Bcl-2/Bax Proteins in Drug Resistance. *Oncogene* **1996**, *12*, 1055−1062.
(26) Nita, M. E.; Nagawa, H.; Tominaga, O.; Tsuno, N.; Fujii, S.; Sasaki, S.; Fu, C. G.; Takenoue, T.; Tsuruo, T.; Muto, T. 5-fluorouracil Induces Apoptosis in Human Colon Cancer Cell Lines with Modulation of Bcl-2 Family Proteins. *Br. J. Cancer* **1998**, *78*, 986−992.
(27) Tas, F.; Duranyildiz, D.; Argon, A.; Oguz, H.; Camlica, H.; Yasasever, V.; Topuz, E. Serum Bcl-2 and Survivin Levels in Melanoma. *Melanoma Res.* **2004**, *14*, 543−546.
(28) Li, L. L.; Wu, G. H.; Hong, T.; Yin, Z. Y.; Sun, D.; Abdel-Halim, E. S.; Zhu, J. J. Graphene Quantum Dots as Fluorescence Probes for Turn-off Sensing of Melamine in the Presence of Hg^{2+}. *ACS Appl. Mater. Interfaces* **2014**, *6*, 2858−2864.
(29) Chen, X. C. Core/shell Structured Silica Spheres with Controllable Thickness of Mesoporous Shell and its Adsorption, Drug Storage and Release Properties. *Colloids Surf., A* **2013**, *428*, 79−85.
(30) Lu, F.; Zhou, S. W.; Zhu, J. J. Photochemical Synthesis of Fluorescent Ag Nanoclusters and Enhanced Fluorescence by Ionic Liquid. *Int. J. Hydrogen Energy* **2013**, *38*, 13055−13061.
(31) Li, L. L.; Chen, Y.; Lu, Q.; Ji, J.; Shen, Y. Y.; Xu, M.; Fei, R.; Yang, G. H.; Zhang, K.; Zhang, J. R.; Zhu, J. J. Electrochemiluminescence Energy Transfer-promoted Ultrasensitive Immunoassay Using Near-infrared-emitting CdSeTe/CdS/ZnS Quantum Dots and Gold Nanorods. *Sci. Rep.* **2013**, *3*, 1−10.
(32) Shi, J. J.; He, T. T.; Jiang, F.; Abdel-Halim, E. S.; Zhu, J. J. Ultrasensitive Multi-analyte Electrochemical Immunoassay Based on GNR-modified Heated Screen-printed Carbon Electrodes and PS@PDA-metal Labels for Rapid Detection of MMP-9 and IL-6. *Biosens. Bioelectron.* **2014**, *55*, 51−56.
(33) Wang, J. Nanoparticle-Based Electrochemical Bioassays of Proteins. *Electroanalysis* **2007**, *19*, 769−776.
(34) Levicky, R.; Herne, T.; Tarlov, M.; Satija, S. Using Self-assembly to Control the Structure of DNA Monolayers on Gold: a Neutron Reflectivity Study. *J. Am. Chem. Soc.* **1998**, *120*, 9787−9792.
(35) Liu, G. D.; Wang, J.; Kim, J.; Jan, M. R.; Collins, G. E. Electrochemical Coding for Multiplexed Immunoassays of Proteins. *Anal. Chem.* **2004**, *76*, 7126−7130.
(36) Hanson, J. A.; Wang, J.; Kawde, A.-N.; Xiang, Y.; Gothelf, V. K.; Collins, G. Quantum-Dot/Aptamer-Based Ultrasensitive Multi-Analyte Electrochemical Biosensor. *J. Am. Chem. Soc.* **2006**, *128*, 2228−2229.

DOI: 10.1021/acsami.6b01010
ACS Appl. Mater. Interfaces 2016, 8, 7674−7682

(37) Yang, C.; Xu, C. X.; Wang, X. M.; Hu, X. Quantum-Dot-Based Biosensor for Simultaneous Detection of Biomarker and Therapeutic Drug: First Steps Towards an Assay for Quantitative Pharmacology. *Analyst* **2012**, *137*, 1205−1209.
(38) Vuki, M.; Shiu, K. K.; Galik, M.; O'Mahony, M. A.; Wang, J. Simultaneous Electrochemical Measurement of Metal and Organic Propellant Constituents of Gunshot Residues. *Analyst* **2012**, *137*, 3265−3270.
(39) Pathak, S.; Sharma, H.; Sharma, C.; Jayaram, N. H.; Singh, N. Apoptotic Signaling Induced by Tiazofurin-an in Vitro Study. *Gene Ther. Mol. Biol.* **2006**, *10*, 199−206.
(40) Meruvu, S.; Zhang, J.; Bedi, S. Y.; Choudhury, M. Mono-(2-ethylhexyl) Phthalate Induces Apoptosis through miR-16 in Human First Trimester Placental Cell Line HTR-8/SVneo. *Toxicol. In Vitro* **2016**, *31*, 35−42.
(41) Adefolaju, A. G.; Theron, E. K.; Hosie, J. M. Effects of HIV Protease, Nucleoside/Non-Nucleoside Reverse Transcriptase Inhibitors on Bax, Bcl-2 and Apoptosis in Two Cervical Cell Lines. *Biomed. Pharmacother.* **2014**, *68*, 241−251.
(42) Zhou, S. W.; Zheng, T. T.; Chen, Y. F.; Zhang, J. J.; Li, L. T.; Lu, F.; Zhu, J. J. Toward Therapeutic Effects Evaluation of Chronic Myeloid Leukemia Drug: Electrochemical Platform for Caspase-3 Activity Sensing. *Biosens. Bioelectron.* **2014**, *61*, 648−654.
(43) Xu, Y.; Bai, H.; Lu, G.; Li, C.; Shi, G. Flexible Graphene Films via the Filtration of Water-soluble Noncovalent Functionalized Graphene Sheets. *J. Am. Chem. Soc.* **2008**, *130*, 5856−5857.
(44) Li, D.; Muller, M. B.; Gilje, S.; Kaner, R. B.; Wallace, G. G. Processable Aqueous Dispersions of Graphene Nanosheets. *Nat. Nanotechnol.* **2008**, *3*, 101−105.
(45) Hummers, W. S.; Offeman, R. E. Preparation of Graphitic Oxide. *J. Am. Chem. Soc.* **1958**, *80*, 1339−1339.
(46) Kim, J.; Kim, H. S.; Lee, N.; Kim, T.; Kim, H.; Yu, T.; Song, I. C.; Moon, W. K.; Hyeon, T. Multifunctional Uniform Nanoparticles Composed of a Magnetite Nanocrystal Core and a Mesoporous Silica Shell for Magnetic Resonance and Fluorescence Imaging and for Drug Delivery. *Angew. Chem., Int. Ed.* **2008**, *47*, 8438−8441.
(47) Yu, X. W.; Sheng, K. X.; Chen, J.; Li, C.; Shi, G. Q. Electrochemical Biosensing Based on Graphene Modified Electrodes. *Huaxue Xuebao* **2014**, *72*, 319−332.
(48) Abergel, D. S. L.; Apalkov, V.; Berashevich, J.; Ziegler, K.; Chakraborty, T. Properties of Graphene: A Theoretical Perspective. *Adv. Phys.* **2010**, *59*, 261−482.
(49) Guo, H. L.; Wang, X. F.; Qian, Q. Y.; Wang, F. B.; Xia, X. H. A Green Approach to the Synthesis of Graphene Nanosheets. *ACS Nano* **2009**, *3*, 2653−2659.
(50) Yakovlev, G. A.; Faden, I. A. Caspase-Dependent Apoptotic Pathways in CNS Injury. *Mol. Neurobiol.* **2001**, *24*, 131−144.
(51) Budd, C. R. Activation-Induced Cell Death. *Curr. Opin. Immunol.* **2001**, *13*, 356−362.
(52) Zhou, S. W.; Kong, Y.; Shen, Q. M.; Ren, X. L.; Zhang, J. R.; Zhu, J. J. Chronic Myeloid Leukemia Drug Evaluation Using a Multisignal Amplified Photoelectrochemical Sensing Platform. *Anal. Chem.* **2014**, *86*, 11680−11689.

DOI: 10.1021/acsami.6b01010
ACS Appl. Mater. Interfaces 2016, 8, 7674−7682